INSTITUTE OF PHYSICS PUBLISHING JOURNAL OF PHYSICS D: APPLIED PHYSICS

J. Phys. D: Appl. Phys. **38** (2005) 2952–2966 doi:10.1088/0022-3727/38/16/032

Monte Carlo studies of electron transport in crossed electric and magnetic fields in CF_4

S Dujko, Z M Raspopović and Z Lj Petrović

Institute of Physics, PO Box 68, 11080 Zemun, Serbia and Montenegro

Received 13 January 2005, in final form 18 May 2005
Published 5 August 2005
Online at stacks.iop.org/JPhysD/38/2952

Abstract

Electron transport in crossed electric and magnetic dc fields in CF_4 is considered by employing an exact Monte Carlo simulation technique. Emphasis is placed on explicit and implicit effects of the combination of both the shape of cross-sections and magnetic field on relaxation processes and steady-state transport data. It has been shown that the application of a magnetic field changes the relaxation processes by increasing the relaxation times as well as, by introducing the oscillatory behaviour of some transport quantities during the relaxation process itself. The electron transport parameters studied here are collision frequency, mean energy, drift velocity, diffusion tensor and collisional rates for $1 \leqslant E/N \leqslant 1000$ Td and $0 \leqslant B/N \leqslant 1000$ Hx ($1\,\text{Td} = 10^{-21}\,\text{V m}^2$, $1\,\text{Hx} = 10^{-27}\,\text{T m}^3$). Special attention is paid to the study of sensitivity of transport data in $\boldsymbol{E} \times \boldsymbol{B}$ fields on the energy dependence and nature of the cross-sections. The validity of the effective reduced electric field concept through Tonks' theorem is also investigated for CF_4 in the evaluated range of mean energies.

1. Introduction

Over the past few decades, there has been considerable research on electron swarms in a neutral gas in the presence of electric and magnetic fields. This interest was intensified owing to the broad range of applications of non-equilibrium (low temperature) plasmas with both electric and magnetic fields. With respect to this, the most common situations involve orthogonal configuration of electric and magnetic fields. These applications range from magnetically confined gas lasers to high-energy particle detectors and to plasma processing technology involving magnetically enhanced plasma reactors.

Studies of the application of a magnetic field perpendicular to the electric field on the electron transport date back many years. The first experiments in crossed electric and magnetic dc fields were conducted by Townsend and Tizard in 1913 [1] and by Huxley and Zaazou in 1949 [2]. They measured electron swarm parameters in the regime where the electron cyclotron frequency is much smaller than the electron collision frequency ($\Omega \ll \nu_c$). On the other hand, Bernstein [3] measured the electron swarm coefficients in the regime where cyclotron frequency is much larger than the collision frequency ($\Omega \gg \nu_c$). In addition, one of the most striking phenomena that have been observed is the dramatic influence of the magnetic field on the breakdown voltage in some gases. Application of a magnetic field may reduce the breakdown voltage from tens of kilovolts to a few hundred volts [4]. These and other early attempts (before the 1980s), both experimental and theoretical, to include magnetic fields in gas discharge processes and electron transport have been reviewed by Huxley and Crompton [5] and also by Heylen [6].

The 1980s brought new challenges. Some illustrative examples of electron transport studies in $\boldsymbol{E} \times \boldsymbol{B}$ fields that date back to the 1980s and early 1990s fall into the following categories: (i) modelling of gas lasers, in particular CO_2 lasers [7, 8]; (ii) modelling of a cathode fall region [9, 10]; (iii) modelling of the high-energy particle detectors [11, 12]; and (iv) swarm analyses in sulphur hexafluoride (SF_6) [13–15], in nitrogen (N_2) [16, 17] and in mercury vapour [18]. In all cases, except [8, 11, 12], the Monte Carlo method was employed in order to study the effect of the magnetic field on electron transport and, consequently, the features of gas discharges. Shimura and Makabe [19] analysed velocity distribution function of electrons in $\boldsymbol{E} \times \boldsymbol{B}$ fields in argon by direct numerical analysis of the Boltzmann equation by using the finite element method. In addition, Biagi [20] has recently

developed a Monte Carlo simulation code in order to determine the electron transport parameters in $\boldsymbol{E} \times \boldsymbol{B}$ fields in counting gas mixtures while Raspopović *et al* [21] have presented detailed benchmark calculations in $\boldsymbol{E} \times \boldsymbol{B}$ fields.

Besides the Monte Carlo simulation technique of studying the electron transport, another well-known method is by solving the Boltzmann equation. In the 1980s the main approach to solving the Boltzmann equation was based on using the two term approximation. In order to overcome the limitations of the two term approximation, Biagi [11, 12] extended the two term theory while Ikuta and Sugai [22] developed the 'flight time integral' method for the Boltzmann equation for both perpendicular and orthogonal field configurations. The latter method was associated with an error in the definition of diffusion, as calculations in model gases based on the momentum transfer theory [23], on the multi-term moment method [24] and the Monte Carlo simulation [25] have shown.

Despite the fact that the plasma community, especially plasma modellers, require a lot of transport data, the experimental work on electron transport in $\boldsymbol{E} \times \boldsymbol{B}$ fields is extremely limited. Numerous studies were carried out within the particle detector community [26–28] that were seldom cross-referenced in the swarm community. A glaring exception is the group from Hidelberg (Germany) that has designed the experiment to measure the electron transport parameters in both, the collision-dominated regime, and the regime where magnetic field controls the behaviour of the electron swarm with uncertainty of less than 1% [29, 30]. In addition, one ought to mention the experiments based on the 'photon flux' technique conducted by Brennan and Garvie [31] in order to measure the electron transport parameters in Townsend discharges in nitrogen.

On the other hand, Ness and co-workers have extended the traditional multi-term kinetic theory that considered only electric fields. In [32] Ness developed a formal theory based on the spherical-decomposition of the swarm particle velocity distribution function in the presence of electric and magnetic fields. Within the framework of this theory, Ness [24] presented results for electron swarms for a range of model and real gases. Further improvements of this theory were made by White *et al* [33–35] by developing an extension of the numerical solution of the conservative Boltzmann equation to arbitrary angles between the electric and magnetic fields and by Ness and Makabe [36], by including the effects of non-conservative collisions in $\boldsymbol{E} \times \boldsymbol{B}$ fields. The work of Ness and co-workers is the most comprehensive, accurate and detailed of all the studies done on electron transport in crossed electric and magnetic fields in the literature.

In the physical understanding of electron transport in $\boldsymbol{E} \times \boldsymbol{B}$ fields, approximate theories such as the momentum transfer theory have also been important. Within the framework of this theory, it is possible to obtain analytically the hydrodynamic electron transport coefficients. In the case of electron transport in $\boldsymbol{E} \times \boldsymbol{B}$ fields, momentum transfer theory was developed by Robson [37] but only for conservative electron-neutral collisions. An extension to a more general non-conservative case was made by Vrhovac and Petrović [38, 39] as well as by Li *et al* [40].

In this paper we have employed a Monte Carlo simulation code to study electron transport in $\boldsymbol{E} \times \boldsymbol{B}$ fields in carbon tetrafluoride (CF_4). Initially, our attention is focused on relaxation processes of the energy distribution function (EEDF) and electron transport coefficients. The relaxation problem is analysed for the carefully selected electric and magnetic field strengths in order to cover both regimes of the electron swarm behaviour: the collision-dominated regime and the magnetic field-controlled regime. We have calculated the relaxation times of the EEDF and electron swarm coefficients and compared these results with those that arise from a traditionally kinetic approach. These studies are highly relevant for plasma modellers since fluid theories such as the relaxation continuum theory (RCT) require the knowledge of both relaxation times of electron transport coefficients and rate coefficients [41]. In particular, we have studied the modifications of the relaxation processes in $\boldsymbol{E} \times \boldsymbol{B}$ fields and compared these results with the magnetic field-free case.

Next, we present the steady-state electron transport coefficients for various magnetic and electric fields with a particular emphasis on the effects of non-conservative collisions. In addition, we give a brief description of the magnetic field effect on electron transport properties in $\boldsymbol{E} \times \boldsymbol{B}$ fields in terms of the ratio of the cyclotron to the collision frequency. Finally, owing to the additional numerical complexity by introducing the magnetic field in both Monte Carlo simulation codes and multi-term codes for solving the Boltzmann equation, one may be forced to employ the effective field concept [42]. According to the effective field concept, one may use data obtained from calculations that involve only electric fields that are modified to represent the effect of magnetic fields, mainly on the mean energy [43, 44], and we have tested this approximation.

CF_4 has all the features of the cross-sections that are of great consequence for electron transport [45]. Here it is of interest to establish how they affect the transport properties in the presence of magnetic fields and also possibly to predict how they affect the performance of plasma reactors. Finally, in addition to the published papers that concern both experimental data [46] and swarm analysis in the electric field only [47–50], the numerical modelling performed here in $\boldsymbol{E} \times \boldsymbol{B}$ fields can be useful for comprehensive modelling of a wide range of CF_4 discharges including dc discharges [51–53], rf and microwave discharges [54–56], studies of gas discharge opening switches [57] and technology of gaseous dielectrics [58].

CF_4 is one of the most frequently used gases in plasma applications in ultra large scale integrated (ULSI) circuit technologies for plasma etching. These applications are mostly realized in capacitively coupled plasmas (CCP). Since this paper is concerned with the effect of magnetic field on transport, it is of interest in this context to state that CF_4 was also used in inductively coupled plasmas (ICP) in single, two frequency as well as in pulsed regimes [59]. Thus, it is highly desirable to study electron transport in $\boldsymbol{E} \times \boldsymbol{B}$ fields and provide data for optimal control and design of plasma reactors that may be developed.

2. Technique of simulation

In this paper we apply a Monte Carlo simulation code that follows a large number of electrons (typically 10^4–10^6) through a neutral gas under the influence of uniform and

crossed electric and magnetic fields. It is assumed that an electron swarm develops in an infinite space. At time $t = 0$, electrons are initially released from the origin with the Maxwellian velocity distribution and with a mean kinetic energy of 1 eV. Electrons gain the energy from the external electric field and dissipate it by collisions with the neutral gas molecules. The collisional transfer of this energy to the neutral gas molecules occurs by means of elastic as well as different types of inelastic collisions. It is also assumed that the electron density is sufficiently small, so Coulomb interactions between the particles as well as shielding of the field is negligible. All calculations were performed for zero gas temperature.

2.1. Electron trajectory in $\boldsymbol{E} \times \boldsymbol{B}$ fields

In this work, our coordinate system is defined such that the applied electric field is in x direction while the magnetic field is in the z direction. However, in our final notation we shall use subscripts $\boldsymbol{E}$, $\boldsymbol{B}$ and $\boldsymbol{E} \times \boldsymbol{B}$ to denote the three axes in a more obvious way. The equation of electron motion may be written as

$$m_{\mathrm{e}} \frac{\mathrm{d}\boldsymbol{v}}{\mathrm{d}t} = e(\boldsymbol{E} + \boldsymbol{v} \times \boldsymbol{B}), \tag{1}$$

$$\frac{\mathrm{d}\boldsymbol{r}}{\mathrm{d}t} = \boldsymbol{v}, \tag{2}$$

where m_{e} is the mass of electron, e is the electronic charge, $\boldsymbol{v}$ is the velocity of electron and $\boldsymbol{E}$ and $\boldsymbol{B}$ are the electric and magnetic fields, respectively. The classical, finite difference method of numerical integration for equations (1) and (2) may be expressed by

$$\boldsymbol{v}(t + \Delta t) = \boldsymbol{v}(t) + \frac{e}{m_{\mathrm{e}}}(\boldsymbol{E} + \boldsymbol{v} \times \boldsymbol{B})\Delta t, \tag{3}$$

$$\boldsymbol{r}(t + \Delta t) = \boldsymbol{r}(t) + \boldsymbol{v}(t + \Delta t)\Delta t. \tag{4}$$

The classical, numerical procedure of solving equations (3) and (4) is not time consuming, but it gives unsatisfactorily results for the electron position and velocity in $\boldsymbol{E} \times \boldsymbol{B}$ fields. That is, if we assume $\boldsymbol{E} = 0$ we will not get a closed circle in numerical solution for an electron trajectory owing to the change of velocity during Δt. Therefore, we have employed Boris rotation, a well-known algorithm in plasma physics for electron motion in $\boldsymbol{E} \times \boldsymbol{B}$ fields [60]. It is based on the use of the electric field only. After each time step, the electron velocity is rotated in such a way as to obtain the effect of a magnetic field. The angle of rotation is dependent on the magnitude of the magnetic field. According to this procedure, the additional velocities were introduced as follows:

$$v_x' = v_x + tg\left(-\frac{\theta}{2}\right) v_y, \tag{5}$$

$$v_y' = v_y - tg\left(-\frac{\theta}{2}\right) v_x, \tag{6}$$

where v_x and v_y are the current components of electron velocities with a time step of $\Delta t/2$, and θ is given by

$$\theta = \frac{eB}{m}\Delta t. \tag{7}$$

Since the magnetic field is oriented along the z axis, the new components of the drift velocity are obtained by the following rotation:

$$v_x = v_x + s v_y', \tag{8}$$

$$v_y = v_y - s v_x', \tag{9}$$

where s and t are the parameters of rotation given by

$$t = -tg\left(\frac{\theta}{2}\right), \tag{10}$$

$$s \equiv -\sin\theta = \frac{2t}{1 + t^2}. \tag{11}$$

At the end of this procedure, it is necessary once more to accelerate the electron along the electric field using the time step of $\Delta t/2$.

2.2. Determining the probability and the nature of collisions

The crucial features of a Monte Carlo method of charged particle transport are to follow accurately the path of an individual electron and to determine the exact moment and the nature of the next electron collision. The probability that the electron has no collision before the time t is given by

$$P(t) = \exp\left(-\int_{t_0}^{t} \nu_{\mathrm{T}}(\varepsilon(t'))\mathrm{d}t'\right), \tag{12}$$

where t_0 is either the time of the electron entering into gas or the time of a previous collision. The time-dependent total collision frequency ν_{T} is given by

$$\nu_{\mathrm{T}}(\varepsilon(t)) = N\sigma_{\mathrm{T}}(\varepsilon)v, \tag{13}$$

where N is the density of the background molecules, $\sigma_{\mathrm{T}}(\varepsilon)$ is the total collision cross-section and v is the electron velocity. The probability density that the collision occurs in the time interval $(t, t + \mathrm{d}t)$ is given by

$$p(t)\mathrm{d}t = P(t) - P(t + \mathrm{d}t) \tag{14}$$

and hence

$$p(t) = \nu_{\mathrm{T}}(\varepsilon(t)) \exp\left(-\int_{t_0}^{t} \nu_{\mathrm{T}}(\varepsilon(t'))\mathrm{d}t'\right). \tag{15}$$

A random collision time t_{c} may be obtained by equalizing the probability that the random number ξ_1 is from the uniform distribution on the interval $(0, 1)$ and the probability that a random collision time t_{c} is on the interval $[t_0, t_{\mathrm{c}}]$ and hence

$$-\ln(1 - \xi_1) = \int_{t_0}^{t_{\mathrm{c}}} \nu_{\mathrm{T}}(\varepsilon(t))\mathrm{d}t. \tag{16}$$

Equation (16) has no analytical solutions for real gases. There are two methods of solving this equation. The first method is known as *null-collision method*, initially developed by Skullerud [61] for simulation of ion motion in gases. This method has been used extensively for electrons in electric fields [62, 63]. It assumes that an additional process that has no effect on electrons upon collision is added in such a way that the total collision frequency is constant.

The second method, known as the *time integration method* [64, 65], is based on numerical integration of equation (17) in small time steps. According to this method, equation (16) may be written as

$$\ln(1-\xi_1) \leqslant -\sum_i \nu_T(\varepsilon(t_i))\Delta t_i. \tag{17}$$

The sum in the exponent of the inequality (17) is usually known as the collision sum. The essence of this method is to check whether the collision sum becomes greater than the logarithm of a random number. If an inequality (17) does not hold for some Δt_k, the collision occurs and $\sum \Delta t_k$ represents the solution.

It is obvious that the most critical step of the time integration method is to decide how long the time-steps for numerical integration should be. In our code the time steps are determined as the minimum of the two relevant time constants (mean collision time and cyclotron period for $\boldsymbol{E} \times \boldsymbol{B}$ fields) divided by a large number (20–100). Varying the number that is used to divide the time constants gives a test of the convergence of the method itself.

Despite the fact that the null-collision method has an advantage in dc fields we, employ the time integration technique in our Monte Carlo code as we want to apply the same code for rf fields and also to control the accuracy of the electron trajectories in magnetic fields.

The nature of a collision is determined from another uniformly distributed random number ξ_2 between 0 and 1, taking into account the relative probabilities (collision frequencies) of all collisions.

2.3. Determining the scattering parameters

The next step in our Monte Carlo method is to calculate the properties of the electron after the scattering. The change in the direction of the electron velocity is described by an azimuthal angle φ and by the scattering angle θ. The azimuthal angle is assumed to be uniformly distributed in the range $[0, 2\pi]$

$$\varphi = 2\pi\xi_3, \tag{18}$$

where ξ_3 is the new uniformly distributed random number between 0 and 1. The scattering angle may be anisotropically distributed and the probability for the electron with energy ε to be scattered over an angle θ is determined by the differential cross-section $I(\varepsilon, \theta)$. In this paper we assume that all electron scattering is isotropic, regardless of the collision nature, thus a random scattering angle θ may be found simply as

$$\theta = \cos^{-1}(1-2\xi_4), \tag{19}$$

but in that case, momentum summed momentum transfer cross-section should be used instead of the total cross-section for determining the probability of collision. This approximation was generally shown to be adequate for relatively low E/N covered in this paper but needs to be corrected when forward scattering becomes dominant. The effect of anisotropic scattering in the region of the Ramsauer minimum should also be re-considered for a detailed understanding. However, since we attempt to scan a broad range of parameters and to provide a database for plasma modelling, we will not focus on this issue in the present publication.

After an elastic collision, the electron energy is given by

$$\varepsilon_1 = \varepsilon\left[1 - \frac{2m_e}{M}(1-\cos\theta)\right], \tag{20}$$

where ε is the electron energy before the collision, m_e and M are the electron and neutral molecule masses, respectively. On the other hand, the electron energy after an inelastic collision may be easily found by an additional subtraction of the energy loss ε_l from the current total electron energy.

In the case of ionization, the remaining electron energy ε_l is redistributed between the primary and the secondary electron. One may use the approximation that the primary electron takes the whole energy, while the secondary electron starts the motion with zero or the semi-empirical formula initially published by Opal *et al* [66]. Nevertheless, we adopt a concept where the energy of the primary and secondary electron is determined by introducing the new, uniformly distributed random number between 0 and 1, which was shown to be sufficiently accurate in our conditions.

2.4. Sampling the electron transport coefficients and EEDF

When discussing the electron swarms in $\boldsymbol{E}\times\boldsymbol{B}$ fields one should bear in mind that the application of a magnetic field gives rise to additional transport coefficients as compared with the case of a purely electric field. Hence, in the $\boldsymbol{E} \times \boldsymbol{B}$ orthogonal configuration there are drift velocities in $\boldsymbol{E}$ and $\boldsymbol{E}\times\boldsymbol{B}$ directions. D_E, $D_{E\times B}$ and D_B are the components of the diffusion tensor $\boldsymbol{D}$ in $\boldsymbol{E}$, $\boldsymbol{E}\times\boldsymbol{B}$ and $\boldsymbol{B}$ directions, respectively. D_{Hall} is the so-called Hall diffusion coefficient arising from the off-diagonal terms in the diffusion tensor. However, we plot the values of ND coefficients as those are independent of the pressure.

All of these transport coefficients may be defined both in the real and in the velocity space [67]. Usually, the corresponding coefficients are labelled as *bulk* (real space) and *flux* (velocity space) electron transport coefficients [68, 69], respectively. The two sets of coefficients are equal, by definition, in the absence of non-conservative collisions and, conversely, in the presence of non-conservative processes (attachment and/or ionization) they may differ. We use the terminology *'bulk'* and *'flux'* transport coefficients, since appropriate formulae for Monte Carlo simulations that enable a correct representation of non-conservative processes have been presented by Kumar *et al* [67], White *et al* [25] and Nolan *et al* [70]. There is a good agreement of the results with properly defined and calculated real and velocity space coefficients such as those shown by Kurihara *et al* [50]. Proof that the formulae used here concur with those in Boltzmann equation theories is quite complex and beyond the scope of this paper [67]. While it may be more appropriate to use flux coefficients for plasma modelling, the bulk coefficients are measured in swarm experiments.

The bulk electron transport coefficient may be determined from the mean position of the electron swarm in real space. The number changing reaction rate is defined by

$$\omega^{(0)} = -\alpha = \frac{\mathrm{d}}{\mathrm{d}t}(\ln N), \tag{21}$$

the drift velocity by

$$\boldsymbol{\omega}^{(1)} = \boldsymbol{w} = \frac{\mathrm{d}}{\mathrm{d}t}\langle \boldsymbol{r} \rangle, \tag{22}$$

and the diffusion tensor by

$$\boldsymbol{\omega}^{(2)} = \boldsymbol{D} = \frac{1}{2}\frac{\mathrm{d}}{\mathrm{d}t}\langle \boldsymbol{r}^* \boldsymbol{r}^* \rangle, \tag{23}$$

where N is the number of electrons in swarm, $\langle \boldsymbol{r} \rangle$ are electron swarm centre of the mass coordinates and $\boldsymbol{r}^* = \boldsymbol{r} - \langle \boldsymbol{r} \rangle$.

The corresponding flux value for the number changing reaction rate is

$$\Gamma^{(0)} = -\alpha = 0, \tag{24}$$

the drift velocity is

$$\boldsymbol{\Gamma}^{(1)} = \boldsymbol{w} = \langle \boldsymbol{v} \rangle, \tag{25}$$

and the diffusion tensor is

$$\boldsymbol{\Gamma}^{(2)} = \boldsymbol{D} = \frac{1}{2}\left\langle \frac{\mathrm{d}}{\mathrm{d}t}(\boldsymbol{r}^* \boldsymbol{r}^*) \right\rangle, \tag{26}$$

where $\langle \boldsymbol{v} \rangle$ denotes the mean electron velocity of electrons in the swarm.

On the basis of equation (23), and keeping in mind the orientation of the electric and magnetic field vectors, the bulk values of the diagonal components of the diffusion tensor are given by

$$D_E^{\mathrm{bulk}} = \frac{1}{2}\frac{\mathrm{d}}{\mathrm{d}t}(\langle x^2 \rangle - \langle x \rangle^2), \tag{27}$$

$$D_{E\times B}^{\mathrm{bulk}} = \frac{1}{2}\frac{\mathrm{d}}{\mathrm{d}t}(\langle y^2 \rangle - \langle y \rangle^2), \tag{28}$$

$$D_B^{\mathrm{bulk}} = \frac{1}{2}\frac{\mathrm{d}}{\mathrm{d}t}(\langle z^2 \rangle - \langle z \rangle^2). \tag{29}$$

On the other hand, on the basis of equation (26) the flux diffusion coefficients are given by

$$D_E^{\mathrm{flux}} = \langle x V_x \rangle - \langle x \rangle \langle V_x \rangle, \tag{30}$$

$$D_{E\times B}^{\mathrm{flux}} = \langle y V_y \rangle - \langle y \rangle \langle V_y \rangle, \tag{31}$$

$$D_B^{\mathrm{flux}} = \langle z V_z \rangle - \langle z \rangle \langle V_z \rangle. \tag{32}$$

Apart from the diagonal components of the diffusion tensor, as mentioned above, there are off-diagonal components of the diffusion tensor. The Hall diffusion coefficient represents the sum of the off-diagonal components of the diffusion tensor. The bulk value of the Hall diffusion coefficient is given by

$$D_{\mathrm{Hall}}^{\mathrm{bulk}} = \frac{1}{2}\frac{\mathrm{d}}{\mathrm{d}t}(\langle x \rangle \langle y \rangle - \langle xy \rangle). \tag{33}$$

The Hall flux diffusion coefficient is given by

$$D_{\mathrm{Hall}}^{\mathrm{flux}} = \tfrac{1}{2}(\langle x \rangle \langle V_y \rangle + \langle y \rangle \langle V_x \rangle - \langle y V_x \rangle - \langle x V_y \rangle). \tag{34}$$

Bulk transport coefficients are observable quantities that are generally measured and tabulated in swarm experiments. On the other hand, flux transport data may be obtained through Boltzmann analysis. Since there may be considerable differences between these two types of transport data, one should be aware of both origin and type of transport data before their application. In section 3.4, we will examine and estimate the significance of the influence of non-conservative collisions on electron transport in $\boldsymbol{E} \times \boldsymbol{B}$ fields.

The rate coefficients (including the attachment and ionization) may be determined by counting the appropriate collision events and normalizing the count by the time step and number of electrons.

In addition to transport and rate coefficients, we may also determine the EEDF. This may be done by sampling the energy of electrons at fixed moments. However, we have not employed the EEDF to calculate rates and transport coefficients. If one uses Monte Carlo simulated EEDF to integrate and give transport coefficients, we would have to sample all the components in gradient and spherical harmonic expansions in order to use proper formulae. This may then be subject to a large uncertainty owing to poor statistics or biased sampling. Thus, we believe that it is best and certainly most efficient, statistically, to sample the transport coefficients directly.

3. Results and discussion

The electron swarm parameters are calculated for E/N values from 1 to 1000 Td (1 Td $= 10^{-21}$ V m^2) with B/N values in the interval of $0 \leqslant B/N \leqslant 1000$ Hx (1 Hx $= 10^{-27}$ T m^3). The initial number of electrons and simulation time depend on both E/N and B/N. Usually, we follow 10^5 electrons through approximately the same number of collisions. However, at the lowest E/N and the highest B/N owing to many circular rotations per collision and low energy exchange, we used the lowest number of 0.5×10^5 initial electrons. Under the same conditions, the simulation times were the longest, and consequently our simulations took several days on fast desktop computers to complete. The gas number density is 3.54×10^{22} m^{-3}, which corresponds to the pressure of 1 Torr at 273 K.

We have chosen a set of cross-sections for CF_4 published by Kurihara *et al* [50], which has been systematically tested in our laboratory [71] and shown in figure 1. This set of electron-CF_4 cross-sections includes 16 collision processes: elastic momentum transfer (1), three vibrational (2–4) and one electronic excitation cross-section (5), attachment cross-section (6) and also seven dissociative ionization cross-sections (7–13) and three cross-sections for the neutral dissociation (14–16). The difference between this set and that of Christophorou *et al* [46] is that Kurihara *et al* use adjustments of ground state dissociation to fit the ionization rate, while Christophorou and co-workers [48] have allocated almost 5 eV energy loss to the second vibrational resonance at higher energies, and this part of the vibrational cross-section was adjusted to fit the ionization coefficient. Our results for transport coefficients are in very good general agreement with those of Kurihara *et al* [50], and we shall not make comparisons here as we may lose the focus of our study, which is to analyse the effects of magnetic field on electron transport.

3.1. Electron motion in $\boldsymbol{E} \times \boldsymbol{B}$ fields

The basic phenomenology of electron transport in $\boldsymbol{E} \times \boldsymbol{B}$ fields may be expressed in terms of the ratio of the cyclotron to the

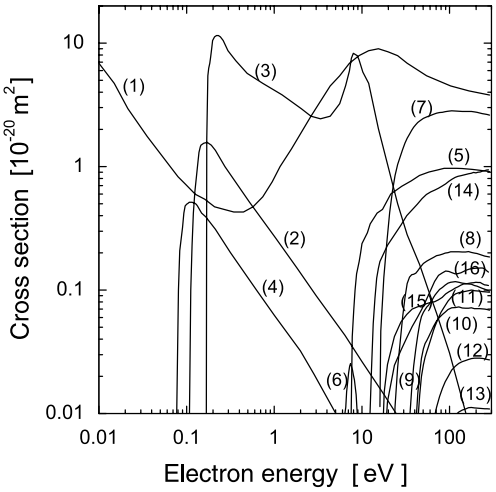

Figure 1. The cross-sections for CF_4 published by Kurihara *et al* [50] including elastic momentum transfer (1), three vibrational (2–4) and one electronic excitation cross-section (5), attachment cross-section (6), seven dissociative ionization cross-sections (7–13) and three cross-sections for the neutral dissociation (14–16).

collision frequency [21, 25]. According to this, there are three regions of importance. First, there is a weak magnetic field region where cyclotron frequency is much smaller than the collision frequency ($\Omega \ll \nu_c$). This indicates that electrons, on average, may complete only a part of their circular orbits between two successive collisions. This regime is called the collision-dominated regime. Second, there is a moderate magnetic field region where cyclotron frequency is of the order of collision frequency ($\Omega \sim \nu_c$). Finally, there is a strong magnetic field region where cyclotron frequency is much larger than the collision frequency ($\Omega \gg \nu_c$). In a strong magnetic field region, electrons may complete many circular orbits per collision, and this regime is known as the magnetic field-controlled regime. In the intermediate magnetic field region, the motion of an electron swarm is complex, inducing certain interesting trends of electron transport coefficients which will be addressed in the following. We should also bear in mind the following: the motion of electrons is mainly chaotic, and randomized velocity is much greater than the drift velocity, further all three regions overlap with the standard conditions found in plasma applications that involve magnetic fields.

In figures 2(*a*) and (*b*), we show the total collision frequency and the ratio of the cyclotron to the total collision frequency as a function of E/N from 1 Td to 1000 Td over a range of B/N from 0 Hx to 1000 Hx, respectively. As can be seen, for a magnetic field-free case, the collision frequency increases with E/N. Application of a magnetic field gives the three distinct ranges of behaviour. First, for all values of magnetic fields, the collision frequency decreases as E/N increases, since the momentum transfer cross-section for elastic collision is a monotonically decreasing function of the electron energy in this energy range. It is somewhat surprising that collision frequency in this energy range is almost independent of B/N. Second, there is a region of rapid rise as momentum transfer cross-section starts to increase markedly. Finally, there is a region of slow increase of the collision frequency owing to the fact that inelastic collisions start to exert their influence on an electron swarm.

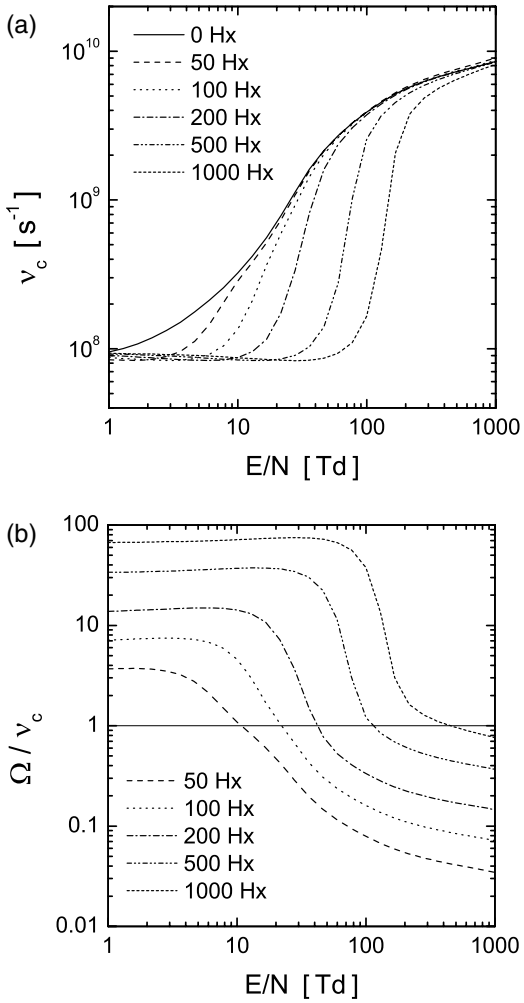

Figure 2. (*a*) Collision frequency and (*b*) the ratio of the cyclotron to the collision frequencies as a function of E/N at various magnetic field strengths.

At fixed values of E/N, the ratio of the cyclotron to the collision frequency increases with increasing B/N, as shown in figure 2(*b*). As B/N increases, the range of E/N where the cyclotron frequency is larger then the collision frequency becomes wider while the transition from the magnetic field-controlled regime to the collision-dominated regime becomes considerably sharper. Thus, with increasing B/N the range of E/N that determines transition from the magnetic field-controlled regime to the collision-dominated regime becomes narrower.

The behaviour of the collision frequency (as a result of the shape of the cross-sections) that we have just described strongly influences the electron transport coefficients. At low B/N, where $\Omega \ll \nu_c$, we may expect a strong influence of collisions and, thereby, a small contribution of the magnetic field. On the other hand, at high B/N and low E/N where $\Omega \gg \nu_c$, owing to the independence of the electron energy capacity of cyclotron rotation, we may expect that the electric field can no longer efficiently pump the energy into the system. In addition, owing to the intensive electron cyclotron motion we may expect reduction of the drift velocity and diffusion coefficients.

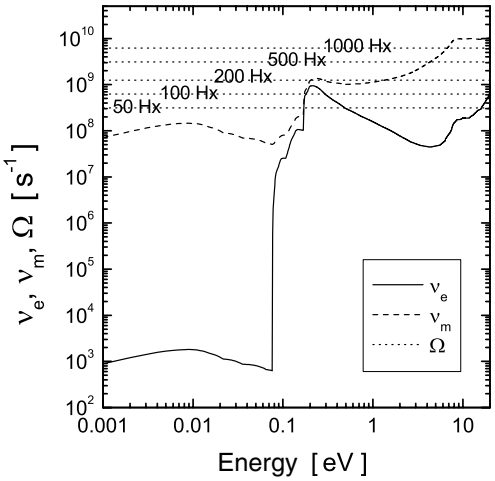

Figure 3. Energy-resolved frequencies for momentum and energy relaxation and cyclotron frequency at various magnetic field strengths.

3.2. Relaxation processes of the EEDF and electron transport coefficients in the $\boldsymbol{E} \times \boldsymbol{B}$ fields

First, we shall discuss the basic features of the temporal relaxation of the EEDF and electron transport coefficients in $\boldsymbol{E} \times \boldsymbol{B}$ fields. Similar studies of both temporal and spatial relaxation processes in neon have already been made by TTA for solving the Boltzmann equation in [72, 73] under the conditions where dominant energy transfer is realized through the electronic excitation. In addition, both studies imply the conservative nature of the Boltzmann collision integral since the ionization was treated as an excitation process.

The basic mechanisms of the relaxation process strongly depend on gas pressure, electric and magnetic fields strengths and the type of gas. In order to study the relaxation processes of an electron swarm, it was common practice to calculate their characteristic parameters such as relaxation times and lengths [72–74]. In figure 3 we show the energy and momentum relaxation frequency as a function of the energy for monoenergetic electrons. These frequencies are compared with the cyclotron frequency for several magnetic field strengths, as indicated on the graph. To calculate both energy resolved momentum and energy relaxation frequencies, we use the following formulae [74]:

$$\nu_{\mathrm{m}}(\varepsilon) = \sqrt{\frac{2}{m_{\mathrm{e}}}}\varepsilon^{1/2}\left(N Q_{\mathrm{m}}(\varepsilon) + \sum_l N Q_l^{\mathrm{tot}}(\varepsilon)\right),$$

$$\nu_{\mathrm{e}}(\varepsilon) = \sqrt{\frac{2}{m_{\mathrm{e}}}}\varepsilon^{1/2}\left(2\frac{m_{\mathrm{e}}}{M} N Q_{\mathrm{m}}(\varepsilon) + \sum_l N Q_l^{\mathrm{tot}}(\varepsilon)\frac{\Delta\varepsilon_l^{\mathrm{tot}}}{\varepsilon}\right),$$

where m_{e}, M, ε, N, Q_{m}, Q_l^{tot}, $\Delta\varepsilon_l^{\mathrm{tot}}$ denote the electron mass, the mass of neutral molecule, the electron energy, the gas number density, the momentum transfer cross-section, the total cross-section and associated energy loss of the lth inelastic collision process.

Both momentum and energy relaxation frequencies show complex energy dependence. Momentum relaxation frequency exceeds the energy relaxation frequency in the whole range of electron energies except around 0.2 eV. In this energy range, owing to the rapid growth of the cross-section for vibrational excitation, the corresponding frequency for energy relaxation jumps sharply by almost 6 orders of magnitude.

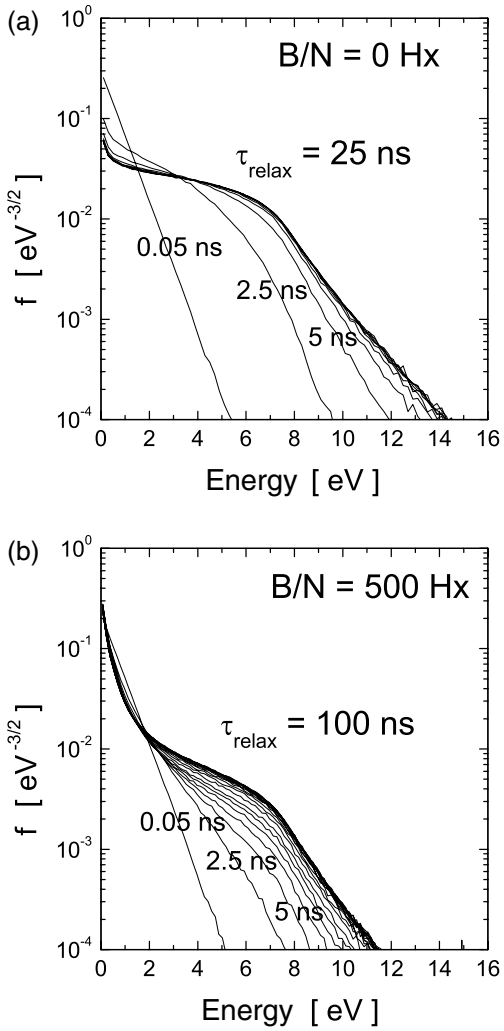

Figure 4. Temporal relaxation of the EEDF for $E/N = 100$ Td at (*a*) $B/N = 0$ Hx and (*b*) $B/N = 500$ Hx.

In figures 4(*a*) and (*b*) we show temporal relaxation of the EEDF, for crossed electric and magnetic fields at $E/N = 100$ Td and B/N of 0 and 500 Hx. As can be seen, application of a magnetic field leads to depopulation of the high-energy electrons from the tail of the EEDF and thereby decreases the mean energy. After 0.05 ns the EEDF is still a Maxwellian (a straight line in the log–lin scale). However, later, the EEDF establishes a non-Maxwellian profile with three distinct energy ranges: (i) low-energy range (ii) intermediate-energy range and (iii) high-energy tail. Transition from low to intermediate-energy range is caused by the fact that electrons are depleted owing to the rapidly rising cross-sections for vibrational excitations. On the other hand, transition from the intermediate to the high-energy range and subsequent cooling of the EEDF starts from approximately 7 eV owing to the new inelastic channels such as electronic excitation and dissociation. Application of a magnetic field changes the speed of the relaxation as well as the shape of the steady-state EEDF. That is, the relaxation time increases with increasing B/N. Also, it is observed that the low-energy range of the EEDF is enhanced as B/N increases.

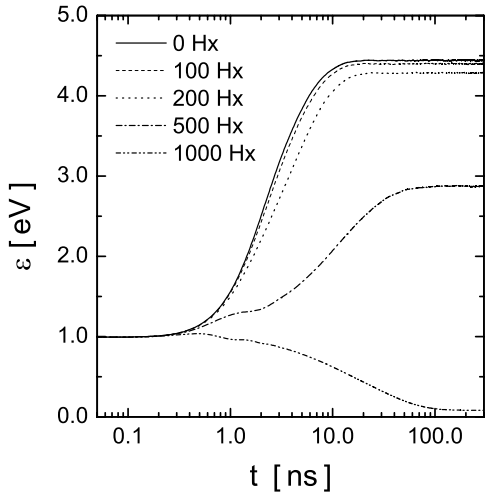

Figure 5. Temporal relaxation of the mean energy for $E/N = 100$ Td and various magnetic fields. The initial energy was arbitrarily chosen to be 1 eV but the final results do not depend on the choice.

In figure 5, we show the temporal relaxation of the mean energy for crossed electric and magnetic fields at $E/N = 100$ Td and $B/N = 0$, 100, 200, 500 and 1000 Hx. The mean energy decreases with B/N for the conditions of the present simulation. At the same time, the relaxation time of the mean energy increases with B/N. This result is caused by the fact that an increase in B/N leads to a weaker energy exchange. On the other hand, the action of the magnetic field decreases the mean energy and shifts it to the range where the energy relaxation frequency is much lower and consequently, the relaxation times increase.

In figures 6(a) and (b) we show the temporal relaxation of the two components of the drift velocity, along the electric field and normal to both electric and magnetic fields, for the same conditions as for the mean energy. In the early stage of relaxation, both components of the drift velocity overshoot the stationary values as a result of rapid acceleration of the initial group of electrons. After a suitable time, drift velocity is decreased towards the stationary value as a consequence of momentum equilibration. In other words, direction of velocity is randomized owing to elastic collisions. Similar effects were observed by Shizgal and McMahon [75] in electron thermalization at low E/N and by Kondo *et al* [76, 77] in rare gases.

3.3. Steady-state electron transport parameters

We now turn our attention to the steady-state transport coefficients in $\boldsymbol{E} \times \boldsymbol{B}$ fields. In figure 7 we show the mean energy as a function of E/N for various B/N. We observe three distinct regions of transport as E/N increases. The first region is associated with slow increases in the mean energy owing to intensive energy losses arising from the vibrational excitation. The second region is that of a rapid rise of mean energy, and it develops when electrons gain sufficient energy to overcome the losses owing to vibrational excitation. It coincides with the negative differential conductivity (NDC) region of the drift velocity, see figure 8. Finally, there is another region of slow increase in the mean energy as the electronic

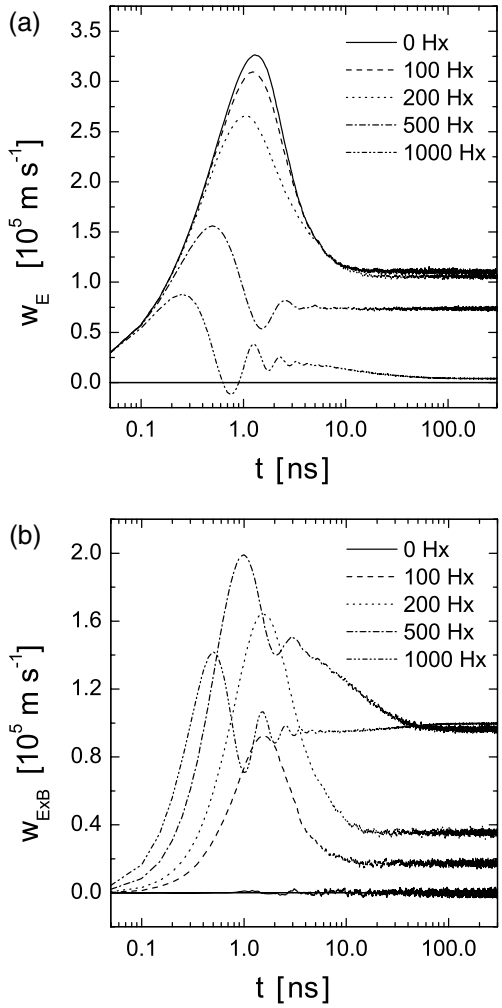

Figure 6. Temporal relaxation of the (a) longitudinal component and (b) perpendicular component of the drift velocity for $E/N = 100$ Td and various magnetic field strengths.

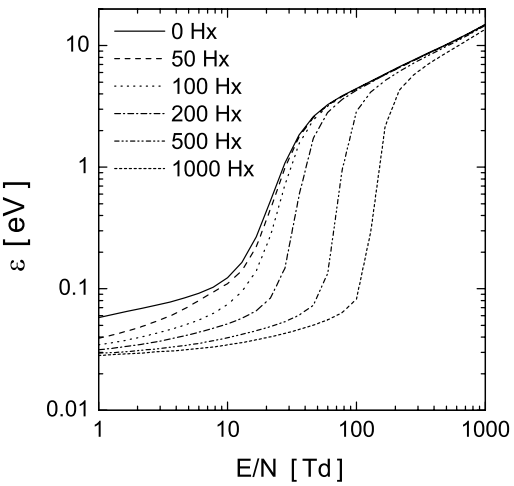

Figure 7. Mean energy as a function of E/N for various B/N.

excitations become important in controlling the energy of the swarm. In general, as can be seen, the application of a magnetic field perpendicular to an electric field decreases the swarm mean energy and, as a result (see figure 7), as

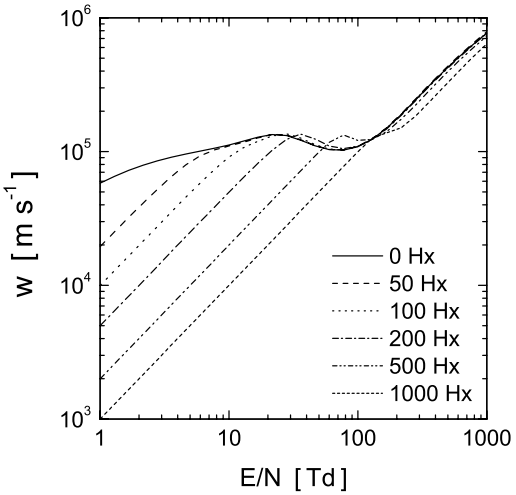

Figure 8. Drift velocity as a function of E/N for various B/N.

B/N increases, the mean energy curves move to the right. In addition, the fastest variation in the mean energy is in the range between 10 and 100 Td where plasma chemistry may be modified significantly by changing the magnitude of an external magnetic field.

In figure 8 we show the magnitude of the vector of drift velocity as a function of E/N for various B/N. It shows a strong effect of NDC which could be expected from the nature of the cross-section [50]. However, as the magnetic field increases from 0 to 500 Hx, the onset of NDC is moving to the right, towards the higher values of E/N. At the highest B/N (covered here) of 1000 Hx, the NDC effect vanishes. As a consequence of such behaviour, there are several points in the range 30–200 Td that show an increase of the drift velocity with increasing B/N. A similar effect was observed in CH_4 [24]. This result is unexpected if one does not take into account the mutual effect on drift velocity by NDC effect and the energy dependent ratio of cyclotron to collision frequency.

At high values of B/N and low values of E/N, e.g. in a magnetic field-controlled regime, drift velocity shows low sensitivity to the details of the cross-section. As can be seen, drift velocity is proportional to E/B, and the curves in figure 8 and also in figure 9 are straight lines. The same is true for the collision-dominated regime, where the curves are again straight lines. The drift velocity is almost insensitive to the presence of a magnetic field at high E/N.

Figures 9(a) and (b) display the longitudinal and perpendicular components of the drift velocity as a function of E/N for various B/N, respectively. As can be seen, the longitudinal component behaves in almost exactly the same way as the magnitude of the vector of the drift velocity with E/N and B/N. It shows a pronounced effect of NDC which disappears at 500 Hx. For each value of B/N, the $\boldsymbol{E} \times \boldsymbol{B}$ component of the drift velocity initially increases with increasing E/N, reaching a peak, and then it starts to decrease with E/N. At the highest E/N (covered in this paper), the drift velocity in the $\boldsymbol{E} \times \boldsymbol{B}$ direction starts to increase again.

In figures 10(a) and (b) we show longitudinal (ND_E) and the transverse component of the diffusion tensor, along the $\boldsymbol{E} \times \boldsymbol{B}$ axis ($ND_{E\times B}$) as a function of E/N for various magnetic fields. At first sight, both diffusion coefficients show a similar

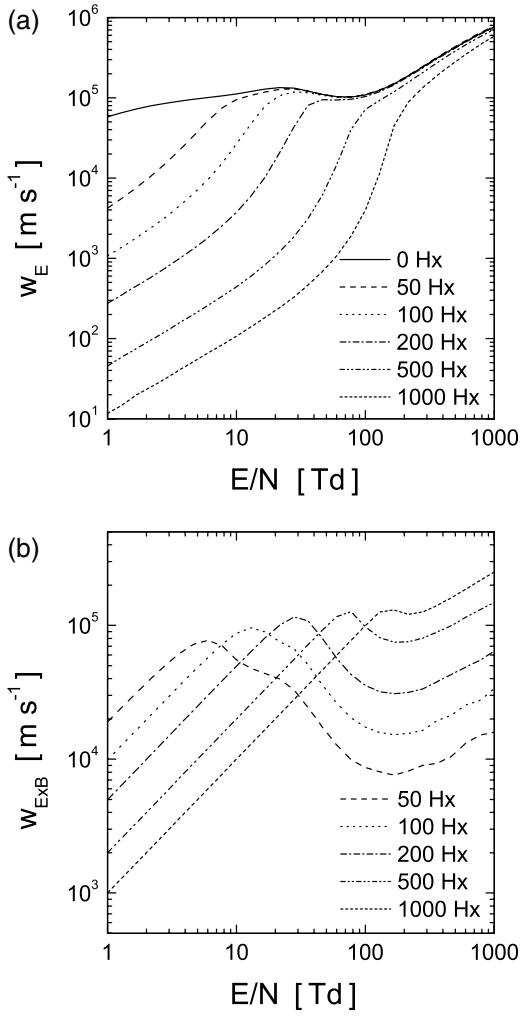

Figure 9. (a) Longitudinal and (b) perpendicular components of the drift velocity as a function of E/N for various B/N.

behaviour with E/N and B/N, particularly in the magnetic field-controlled regime. Both the diffusion coefficients show a rapid rise in the energy range of the Ramsauer–Townsend minimum and rapidly decreasing cross-sections for vibrational excitation. More precisely, both ND_E and $ND_{E\times B}$ may vary over five orders of magnitude with E/N and B/N. In the collision-dominated regime (high E/N), ND_E and $ND_{E\times B}$ are slightly dependent on the presence of a magnetic field. However, in the transition regime, after the rapid rise in their magnitude, both diffusion coefficients show some structures for the case of low B/N values. This indicates an increase in sensitivity to the energy dependence of the cross-sections, particularly to the energy dependence of the cross-sections for vibrational excitation.

In contrast to ND_E and $ND_{E\times B}$, the transverse component of the diffusion tensor along the magnetic field ND_B has much less modulation with both E/N and B/N, as shown in figure 11. Nevertheless, owing to the interplay of the Ramsauer–Townsend minimum and sharply peaked vibrational cross-sections, a structure may be observed and its position moves towards the higher E/Ns with increasing B/N. It is consistent with reduction of energy, in addition, the structure becomes less pronounced and somewhat sharper.

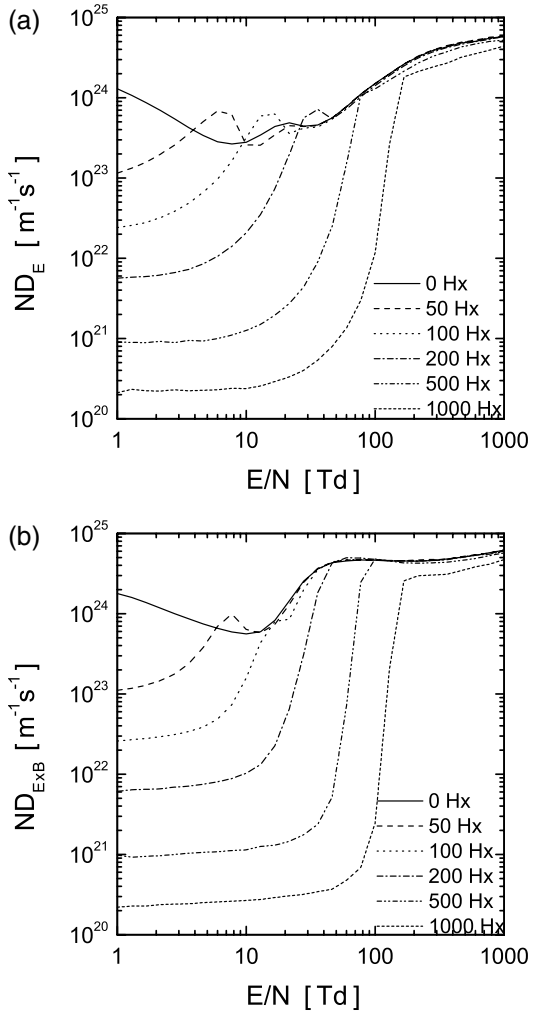

Figure 10. The diffusion coefficients in (*a*) $\boldsymbol{E}$ direction and (*b*) $\boldsymbol{E} \times \boldsymbol{B}$ direction as a function of E/N for various B/N.

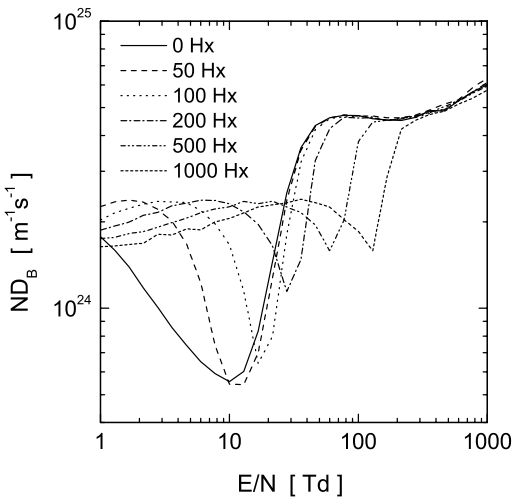

Figure 11. The diffusion coefficient in $\boldsymbol{B}$ direction as a function of E/N for various B/N.

It has been predicted [78] that $\boldsymbol{E} \times \boldsymbol{B}$ component of the diffusion tensor, which is identical to the $\boldsymbol{B}$ component for $\boldsymbol{B} = 0$, changes rapidly and becomes more similar to $\boldsymbol{E}$ component. This was confirmed in the case of CF_4.

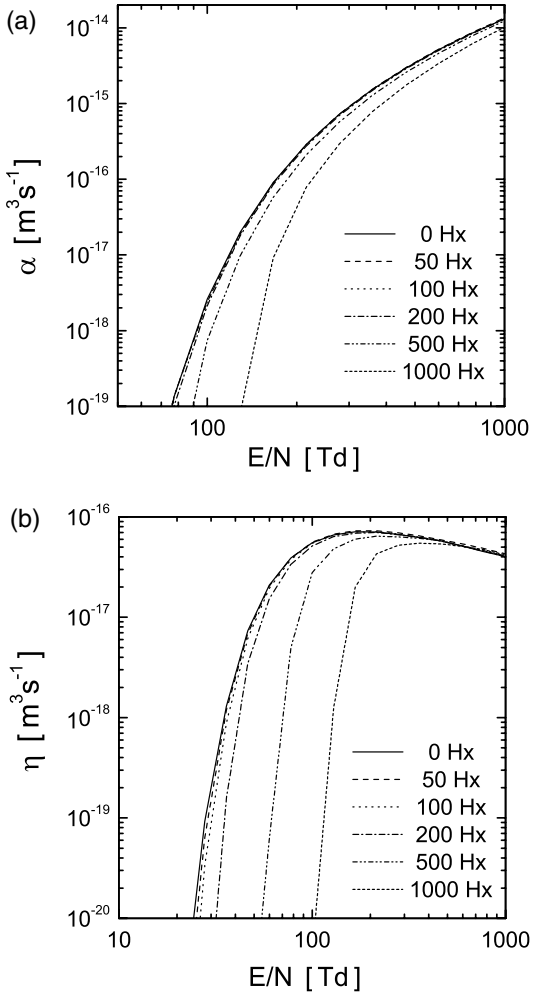

Figure 12. (*a*) Ionization and (*b*) attachment rate coefficients as a function of E/N for various B/N.

In figures 12(*a*) and (*b*) we show the ionization and attachment rate coefficients as a function of E/N for various B/N. As expected, the ionization rate coefficient increases with E/N and decreases with B/N. The attachment rate coefficient has a similar but not identical dependence on E/N and B/N, but the effect of magnetic field is much stronger, as can be expected for a process governed by lower energy electrons.

Figure 13 displays the rate coefficient for dissociation into neutrals with the smallest (k_{d1}) threshold as a function of E/N for various B/N. It behaves with E/N and B/N almost exactly in the same way as the ionization rate coefficient. Again, application of the magnetic field has the smallest effect on the process with the highest threshold.

3.4. The effect of non-conservative interactions on electron transport in the $\boldsymbol{E} \times \boldsymbol{B}$ fields

In this section, we analyse the influence of non-conservative interactions on electron transport in $\boldsymbol{E} \times \boldsymbol{B}$ fields in CF_4. While the difference between various definitions of transport coefficients has been generally neglected in plasma models, we believe that a strong effect of attachment combined with the ionization required to maintain plasma makes this study

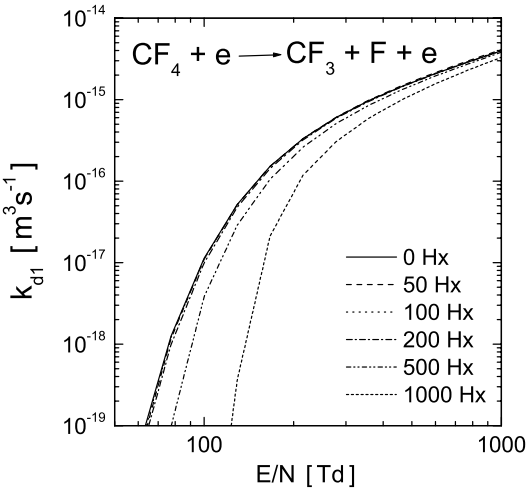

Figure 13. Rate coefficient for dissociation into neutrals with the smallest 0.077 eV threshold as a function of E/N for various B/N.

worthwhile for the $\boldsymbol{E} \times \boldsymbol{B}$ fields in CF_4. We need to stress that while flux data are more appropriate for development of plasma models, often experimental swarm data are used directly and those are, by default, bulk data. The most appropriate procedure would be to use the experimental swarm data for the analysis of the cross-sections and then to calculate the databases for plasma modelling. A similar study has been made by the momentum transfer theory for the ionization and attachment model gases [40].

In figures 14(*a*) and (*b*) we show bulk and flux components of the drift velocity as a function of E/N for B/N of 100 and 1000 Hx. Increasing the magnetic field results in a distinction between bulk and flux transport properties occurring at higher E/N. In particular, for B/N of 100 Hx we may observe a slight but noticeable difference between bulk and flux values of w_E in the range 30–100 Td owing to the attachment. As the ionization becomes stronger, the effect of attachment on w_E becomes weaker and, finally, in the range 140–160 Td there is balancing between the ionization and attachment rate coefficients. It is interesting to note that in this range of E/N, one may expect the minimum of the breakdown voltage for CF_4. Further increase in the electric field leads to a more pronounced difference between the bulk and flux values of w_E, which may be greater then 25%. We observe similar effects for the components of the diffusion tensor.

In contrast to the longitudinal component of the drift velocity, there is no observable effect of the attachment on the transverse component of the drift velocity $w_{E\times B}$, as shown in figure 14(*b*). However, for higher E/N under the conditions where the ionization dominates, we may observe a considerable difference between bulk and flux values of $w_{E\times B}$. Also, in contrast to w_E, in this case the flux values can be larger then the bulk values. This independently confirms a similar result obtained by multi-term procedure for the ionization model gas [79]. It is interesting to note that owing to the assumption of isotropic temperature tensor in momentum transfer theory, the effect of non-conservative interactions could not be observed for $w_{E\times B}$ [40]. Therefore, in order to resolve the difference between bulk and flux components of the drift velocity along the magnetic field in $\boldsymbol{E} \times \boldsymbol{B}$ fields, it is necessary to employ the exact techniques [80].

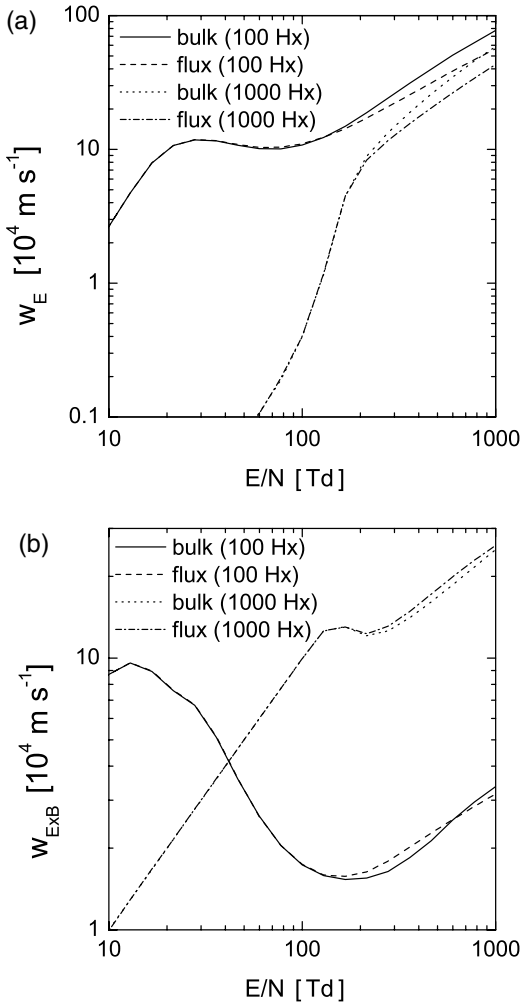

Figure 14. Bulk and flux values of drift velocities in (*a*) $\boldsymbol{E}$ direction and (*b*) $\boldsymbol{E} \times \boldsymbol{B}$ direction as a function of E/N and for B/N of 100 and 1000 Hx.

3.5. Validity of Tonks' theorem

In order to avoid the additional algebraic complexity introduced by the magnetic field in both Boltzmann and Monte Carlo numerical codes, one may be forced to employ the effective field concept. In this approximation, transport in $\boldsymbol{E} \times \boldsymbol{B}$ fields may be described by using a dc electric field that has been modified to include the effect (or at least a partial effect) of magnetic field [71]:

$$E_{\mathrm{eff}}(\varepsilon) = \frac{E}{\sqrt{1 + (\Omega/\nu_{\mathrm{m}})^2}},$$

where E is the real electric field. This approach is known as Tonks' theorem [42–44]. It is obvious that according to Tonks' theorem, the application of a magnetic field to a discharge corresponds qualitatively to an increase in a neutral density (pressure) resulting, eventually, in a lower mean energy. Since the application of Tonks' theorem may be regarded as advantageous for its simplicity, very few tests of its accuracy have been performed and to the best of our knowledge, there were no such tests done in CF_4.

In figures 15(*a*) and (*b*) we show a comparison between the results for the mean energy obtained from our exact

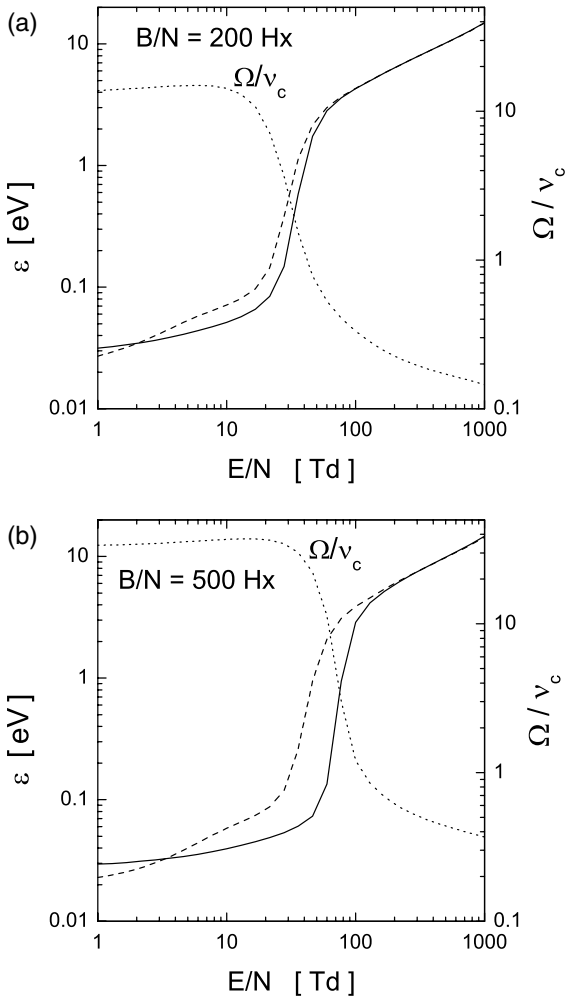

Figure 15. Mean energy as a function of E/N for (*a*) $B/N = 200$ Hx and (*b*) $B/N = 500$ Hx obtained by an exact Monte Carlo calculation (——) and according to Tonks' theorem (- - - -). Dotted line shows the ratio of the cyclotron to the collision frequency.

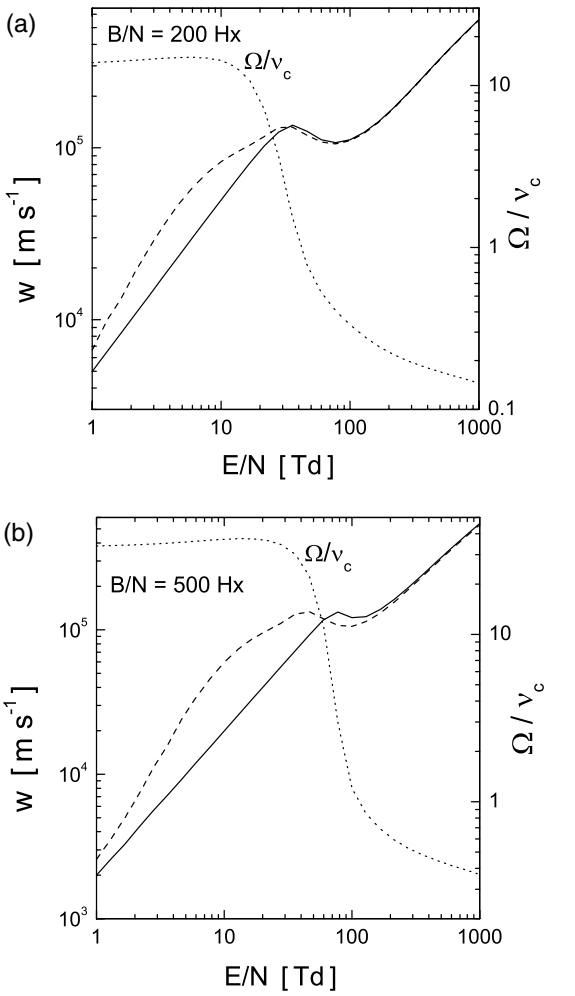

Figure 16. Drift velocity for the same conditions as in figure 15.

Monte Carlo calculations and according to Tonks' theorem for B/N of 200 Hx and 500 Hx, respectively. In figures 16(*a*) and (*b*) we show the comparison for the drift velocity under the same conditions. Similar studies have been shown to be accurate to within 10% for CH_4 over a range of $0.1 \leqslant E/N \leqslant 10$ Td and $0 \leqslant B/N \leqslant 30$ Hx [29]. It is obvious that such a good agreement is obtained under conditions where collision-dominated regime controls the behaviour of an electron swarm. In our case, our calculations have been extended to the magnetic field-controlled regime and have thus provided a wider spectrum of data for a better estimate of the limitation of Tonks' theorem for CF_4.

As expected, the applicability of the effective field concept strongly depends on the ratio of the cyclotron to the collision frequency. In the case of the mean energy and drift velocity (see figures 15(*a*), (*b*) and 16(*a*), (*b*)), we may observe that the effective field concept may be applicable only in the collision-dominated regime. More precisely, if the condition $2\Omega = \nu_c$ holds, the effective field concept is valid. On the other hand, in the magnetic field-controlled regime, the difference between the exact Monte Carlo results and results that follow Tonks' theorem may be one order of magnitude. However, at low values of E/N, we may observe better agreement between these results. This is not connected with the correctness of Tonks' theorem but rather with the fact that in the limit of thermal energies, the influence of a magnetic field is highly reduced as the mean energy cannot be reduced even further.

In figures 17(*a*) and (*b*) we show results for the attachment rate coefficients and in figures 18(*a*) and (*b*) for the ionization rate coefficients. For B/N of 200 Hx we can see an excellent agreement between the results that follow from Tonks' theorem and from exact Monte Carlo calculations. On the other hand, for B/N of 500 Hx, the use of the effective field concept causes larger errors for the attachment rate coefficient with respect to the ionization rate coefficient. This may be explained by the observation that the ionization rate coefficient is due to overlap of the cross-section with the high-energy tail that is least affected by the magnetic field.

4. Conclusion

In this paper, we have presented a systematic investigation of electron transport in CF_4 in crossed electric and magnetic dc fields using a Monte Carlo simulation. We have summarized the basic phenomenology of electron transport in crossed

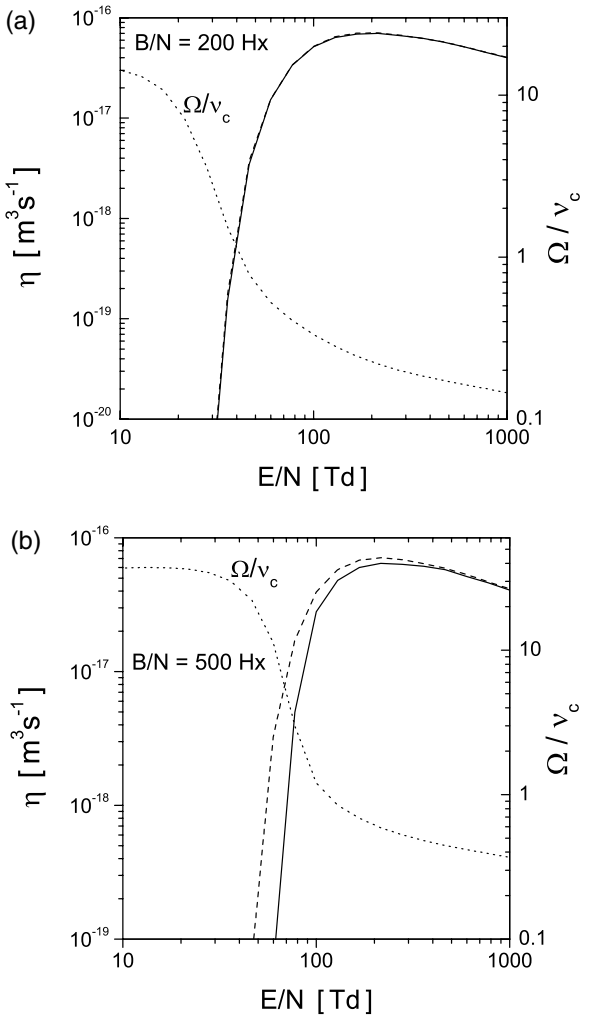

Figure 17. Attachment rate coefficient for the same conditions as in figure 15.

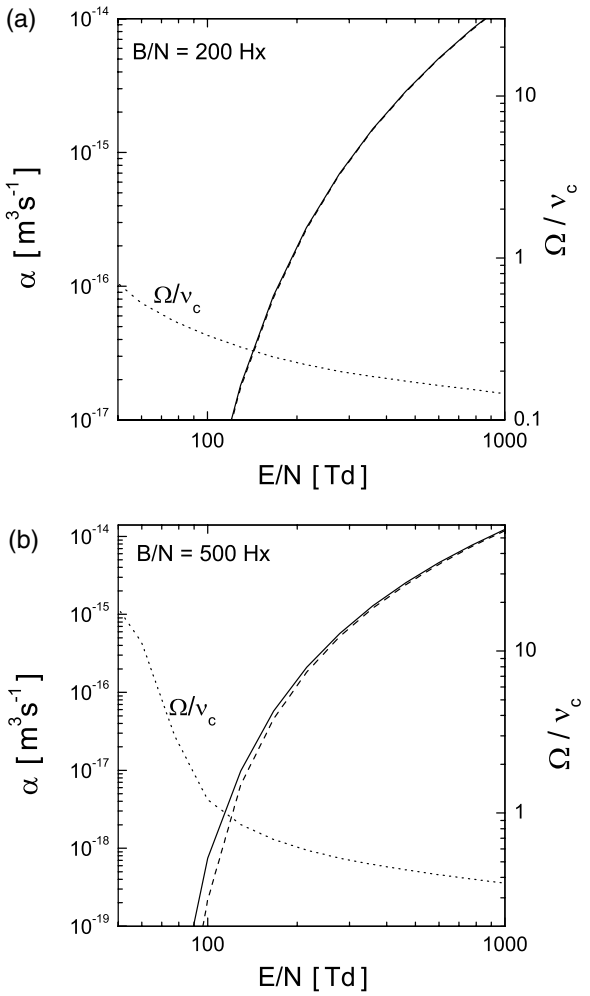

Figure 18. Ionization rate coefficient for the same conditions as in figure 15.

electric and magnetic fields on the basis of the ratio of the cyclotron to the collision frequency. It was found that the application of a magnetic field produces a fast transition from the magnetic field-controlled regime to the collision-dominated regime, which leads to a complex electron kinetics. An example of such complex behaviour of transport data is an increase in the drift velocity at a fixed value of E/N with increasing B/N in the region of NDC.

Relaxation of electron distribution function in crossed electric and magnetic fields has been analysed. It has been shown that temporal relaxation of the electron swarm may be additionally controlled by the application of a magnetic field. Application of a magnetic field changes the speed of relaxation and the shape of the EEDF by depopulation of the high-energy electrons from the tail of the EEDF. The mean energy is reduced while the drift velocity at high values of B/N demonstrates oscillatory behaviour during the relaxation process itself.

The variation of the relaxed (steady-state) transport data with both E/N and B/N has been examined. Application of a magnetic field reduces the mean energy, longitudinal component of the drift velocity and collisional rates. Drift velocity in the $\boldsymbol{E} \times \boldsymbol{B}$ direction at a fixed value of B/N increases with increasing E/N through a maximum and starts to decrease with a further increase of B/N. At the same time, the effect of NDC vanishes in the limit of high magnetic fields. On the other hand, application of the magnetic field introduces complex behaviour of the components of the diffusion tensor. Longitudinal diffusion coefficient ND_E and transverse diffusion coefficient along the $\boldsymbol{E} \times \boldsymbol{B}$ direction may vary over several orders of magnitude with both E/N and B/N. Transverse diffusion coefficient along the magnetic field ND_B shows the highest sensitivity to the energy dependence of the cross-section as compared with other transport coefficients. In general, the sensitivity of the transport coefficients to the energy dependence of the cross-section depends upon the ratio of the cyclotron to the collision frequency. In both, the magnetic field-controlled regime and the collision-dominated regime, the sensitivity of the transport coefficients is diminished with magnetic field.

In this paper, we have also considered the effect of non-conservative collisions, such as ionization and attachment on steady-state transport properties in crossed electric and magnetic fields. Estimates of differences and the origin between bulk and flux values of the transport coefficients have been made.

Finally, we have systematically tested the effective field concept in CF_4 for $\boldsymbol{E} \times \boldsymbol{B}$ fields expressed through Tonks'

theorem. In general, in the collision-dominated regime and in the context of plasma modelling one may use the effective field concept to calculate electron transport data with an acceptable degree of accuracy. However, for more accurate transport data it is necessary to use an exact technique such as the Monte Carlo simulation or multi-term solutions of Boltzmann's equation.

Acknowledgments

The authors are grateful to their co-workers: S Bzenić, S Sakadžić, T Makabe, R D White and R E Robson who participated in our studies of electron transport in dc and rf fields. This work was supported by MNZZS project 1478.

References

[1] Townsend J S and Tizard H T 1913 *Proc. R. Soc.* A **88** 336
[2] Huxley L G H and Zaazou A A 1949 *Proc. R. Soc.* A **88** 402
[3] Bernstein M J 1962 *Phys. Rev.* **127** 335
[4] Harcombe D, Palmer R T and Gozna G F 1963 *J. Sci. Instrum.* **40** 468
[5] Huxley L G H and Crompton R W 1974 *The Diffusion and Drifts of Electrons in Gases* (New York: Wiley)
[6] Heylen A E D 1980 *IEE Proc.* **127** 221
[7] Xu Q-H, Chen Q-M and Li J 1994 *J. Phys. D: Appl. Phys.* **27** 795
[8] Li J and Chen Q-M 1993 *J. Phys. D: Appl. Phys.* **26** 1541
[9] Razdan R, Capjack C E and Seguin H J J 1985 *J. Appl. Phys.* **57** 4954
[10] Li J, Chen Q-M and Li Z-G 1995 *J. Phys. D: Appl. Phys.* **28** 681
[11] Biagi S F 1988 *Nucl. Instrum. Methods* A **273** 533
[12] Biagi S F 1989 *Nucl. Instrum. Methods* A **283** 716
[13] Govinda Raju G R and Dincer M S 1985 *Proc. IEEE* **73** 939
[14] Milsom P K 1993 *J. Phys. D: Appl. Phys.* **26** 237
[15] Dincer M S 1993 *J. Phys. D: Appl. Phys.* **26** 1427
[16] Brennan M J, Garvie A M and Kelly L J 1990 *Aust. J. Phys.* **43** 27
[17] Govinda Raju G R 1990 *IEEE Trans. Plasma Sci.* **18** 819
[18] Liu J and Govinda Raju G R 1992 *J.Phys. D: Appl. Phys.* **25** 465
[19] Shimura N and Makabe T 1993 *Appl. Phys. Lett.* **62** 678
[20] Biagi S F 1999 *Nucl. Instrum. Methods* A **421** 234
[21] Rapopović Z M, Sakadžić S, Bzenić S and Petrović Z Lj 1999 *IEEE Trans. Plasma Sci.* **27** 1241
Petrović Z Lj, Rapopović Z M, Dujko S and Makabe T 2002 *Appl. Surf. Sci.* **192** 1–25
[22] Ikuta N and Sugai Y 1989 *J. Phys. Soc. Japan.* **58** 1228
[23] Robson R E 1994 *Aust. J. Phys.* **47** 279
[24] Ness K F 1994 *J. Phys. D: Appl. Phys.* **27** 1848
[25] White R D, Brennan M J and Ness K F 1997 *J. Phys. D: Appl. Phys.* **30** 810
White R D, Ness K F and Robson R E 2002 *Appl. Surf. Sci.* **192** 26–49
[26] Yamashita T *et al* 1992 *Nucl. Instrum. Methods* A **317** 213
[27] Kiselev O, Prokofiev O and Vorobyov A 1995 *Nucl. Instrum. Methods* A **367** 306
[28] Kirchner J J, Becker U J, Dinner R B, Fidkowski K J and Wyatt J H 2001 *Nucl. Instrum. Methods* A **474** 238
[29] Schmidt B 1993 *Comments At. Mol. Opt. Phys.* **28** 379
[30] Schmidt B, Berkhan K, Goetz B and Mueller M 1994 *Phys. Scr.* T **53** 30
[31] Brennan M J and Garvie A M 1990 *Aust. J. Phys.* **43** 765
[32] Ness K F 1993 *Phys. Rev.* E **47** 327
[33] White R D, Ness K F, Robson R E and Li B 1999 *Phys. Rev.* E **20** 2231
[34] White R D, Ness K F and Robson R E 1999 *J. Phys. D: Appl. Phys.* **32** 1842
[35] White R D, Ness K F and Robson R E 2001 *J. Phys. D: Appl. Phys.* **34** 2205
[36] Ness K F and Makabe T 1999 *Phys. Rev.* E **62** 4083
[37] Robson R E 1994 *Aust. J. Phys.* **47** 279
[38] Vrhovac S B and Petrović Z Lj 1996 *Phys. Rev.* E **53** 4012
[39] Vrhovac S B and Petrović Z Lj 1998 *Electron Kinetics and Application to Glow Discharges* vol 367, ed U Kortshagen and L D Tsendin (New York: Plenum) pp 441–58
[40] Li B, White R D, Robson R E and Ness K F 2001 *Ann. Phys.* **292** 179
[41] Nakano N, Shimura N, Petrović Z Lj and Makabe T 1994 *Phys. Rev.* E **49** 4455
[42] White R D, Robson R E and Ness K F 1999 *IEEE Trans. Plasma Sci.* **27** 1249
[43] Tonks L 1937 *Phys. Rev.* **51** 744
[44] Tonks L and Allis W P 1937 *Phys. Rev.* **52** 710
[45] Tanaka H and Sueoka O 2001 *Advances in Atomic, Molecular and Optical Physics* vol 44, ed M Kimura and Y Itikawa (San Diego: Academic) pp 1–32
[46] Christophorou L G, Olthoff J K and Rao M V V S 1996 *J. Phys. Chem. Ref. Data* **25** 1341
[47] Bordage M C, Segur P and Chouki A 1996 *J. Appl. Phys.* **80** 1325
[48] Bordage M C, Segur P, Christophorou L G and Olthoff J K 1999 *J. Appl. Phys.* **86** 355
[49] Vasenkov A V 2000 *J. Appl. Phys.* **88** 626
[50] Kurihara M, Petrović Z Lj and Makabe T 2000 *J. Phys. D: Appl. Phys.* **33** 2146
[51] Volynets V N, Lukyanova A V, Rakhimov A T, Slovetsky D I and Suetin N V 1993 *J. Phys. D: Appl. Phys.* **26** 647
[52] Slovetsky D I 1990 *Pure Appl. Chem.* **62** 1729
[53] Petrović Z Lj, Raspopović Z M, Dujko S and Makabe T 2002 *Advances in Low Temperature RF Plasmas* ed T Makabe (Amsterdam: Elsevier) pp 1–25
[54] Makabe T and Maeshige K 2002 *Appl. Surf. Sci.* **192** 176–200 and the references therein
Makabe T and Petrović Z Lj 2002 *Appl. Surf. Sci.* **192** 88–114
[55] Metsi E, Gogolides E and Boudouvis A 1996 *Phys. Rev.* E **54** 782
[56] Lisovskiy V A and Yegorenkov V D 1999 *J. Phys. D: Appl. Phys.* **32** 2645
Ohtsu Y, Matsuo H and Fujita H 1996 *Plasma Sources Sci. Technol.* **5** 344
[57] Hunter S R, Carter J G and Christophorou L G 1988 *Phys. Rev.* A **38** 58
[58] Pradazrol C, Casanovas A M, Hernoune A and Casanovas J 1996 *J. Phys. D: Appl. Phys.* **29** 1941
[59] Hioki K, Hirata H, Nakano N, Petrović Z Lj and Makabe T 2000 *J. Vac. Sci. Technol.* A **18** 864
[60] Birdsall C K and Langdon A B 1974 *Plasma Physics Via Computer Simulation* (New York: McGraw-Hill)
[61] Skullerud H R 1968 *J. Phys. D: Appl. Phys.* **1** 1567
[62] Brennan M J, Garvie A M and Kelly L J 1990 *Aust. J. Phys.* **43** 27
[63] Stojanović V D and Petrović Z Lj 1998 *J. Phys. D: Appl. Phys.* **31** 834
[64] Itoh H and Musha T 1960 *J. Phys. Soc. Japan.* **15** 1675
[65] Sakai Y Y, Tagashira M and Sakamoto S 1972 *J. Phys. B: At. Mol. Phys.* **5** 1010
[66] Opal C B, Peterson W K and Beaty E C 1971 *J. Chem. Phys.* **55** 4100
[67] Kumar K, Skullerud H R and Robson R E 1980 *Aust. J. Phys.* **33** 343
[68] Ness K F and Robson R E 1986 *Phys. Rev.* A **34** 2185
[69] Robson R E 1991 *Aust. J. Phys.* **44** 685
[70] Nolan A M, Brennan M J, Ness K F and Wedding A B 1997 *J. Phys. D: Appl. Phys.* **30** 2865
[71] Dujko S, Raspopović Z M and Petrović Z Lj 2003 *BPU-5 Conf. Proc. (Vrnjacka Banja, Serbia and Montenegro, 25–29 August 2003)* (Belgrade: Serbian Physical Society) pp 1017–22

[72] Loffhagen D and Winkler R 1999 *IEEE Trans. Plasma Sci.* **27** 1262
[73] Winkler R, Maiorov V A and Sigeneger F 2000 *J. Appl. Phys.* **87** 2708
[74] Goto N and Makabe T 1990 *J. Phys. D: Appl. Phys* **23** 686–93
Winkler R, Loffhagen D and Sigeneger F 2002 *Advances in Low Temperature RF Plasmas* ed T Makabe (Amsterdam: Elsevier) pp 50–71
[75] Shizgal B and McMahon D R A 1985 *Phys. Rev.* A **32** 3669
[76] Kondo K and Tagashira H 1993 *J. Phys. D: Appl. Phys.* **26** 1948
[77] Kondo K, Fukutoku M, Ikuta N and Tagashira H 1994 *J. Phys. D: Appl. Phys.* **27** 1894
[78] Raspopović Z M, Sakadžić S, Petrović Z Lj and Makabe T 2000 *J. Phys. D: Appl. Phys.* **33** 1298
[79] White R D, Ness K F and Robson R E 2002 *Advances in Low Temperature RF Plasmas* ed T Makabe (Amsterdam: Elsevier) pp 26–49
[80] Robson R E, Hildebrandt M and Schmidt B 1997 *Nucl. Instrum. Methods* A **394** 74